




Improvement on the Structure Design of a Kind of Linear Piezoelectric Motor with Flexible Drive-Foot

Xifu Chen¹ · Ming Li¹ · Huixia Zhang² · Qian Lu¹ · Sungki Lyu³ 

Received: 14 December 2018 / Revised: 13 June 2019 / Accepted: 7 August 2019 / Published online: 13 September 2019
© Korean Society for Precision Engineering 2019

Abstract

Linear piezoelectric motors have wide application prospects in precision instrument, biomedical engineering and many other high technology fields. In this paper, a linear piezoelectric motor operating in non-resonant state was proposed by using a flexible mechanism with characteristics of precision displacement output. Since the stator structural characteristic affects the stability and output performance of the motor directly, this paper focused on the improvement on the structure design of a motor stator with flexible five-bar drive-foot. Firstly, by analyzing the displacement output characteristics of flexible five-bar mechanism, the elliptical trajectory of drive-tip was investigated. Then the drive-foot was particularly designed with the characteristics of flexible structure, and its main structure parameters were improved by the finite element method. Further, the integrated structure of stator was designed and fabricated. Finally, the comparison tests of the two motors were carried out. The experimental results show that the output force and efficiency of the improved piezoelectric motor are increased by 52.38% and 159.15%, respectively.

Keywords Linear motors · Piezoelectric · Flexible drive-foot · Parameter optimization

1 Introduction

Since linear motors can directly output a linear motion without conversion mechanism such as the rack or the pinion mechanism, they have the advantages of compact structure and high output precision. Among them, the linear piezoelectric motor has wide application prospects in biomedical, ultra-precision machining and positioning, aerospace and other fields for its advantages of high positioning accuracy, fast response, good stability and strong anti-interference ability [1, 2]. In recent years, various types of piezoelectric

linear motors have appeared, such as traveling wave type [3], standing wave type [4], acoustic surface wave type [5], inchworm principle type [6], and inertial impact type [7] linear piezoelectric motor.

Many researchers seek to improve the output performance of linear piezoelectric motors by analyzing the characteristics of piezoelectric materials [8], the dynamics of motor systems [9, 10], and the control method of motor systems [11, 12]. Olyai employed the smoothed finite element method in the analysis of piezoelectric effects, and cantilever piezoelectric bimorphs was used to optimize the structural parameter of linear micromotor [13]. Li and Xing used mathematical dynamic optimization to improve the performance of the piezoelectric motor [14]. With the help of the shaking beam, Hyun-Phill Ko found that different tip curves of the motor stator have effects on the parameters, including the actuating force, speed, and electric power of the motor [15]. For the purpose of enhancing the power density of the motor, a u-shaped linear piezoelectric ultrasonic motor stator was proposed by taking use of the longitudinal transducers [16]. Aminzadeh et al. [17, 18] used frame amplifier to improve the piezoelectric actuator performance.

At present, a lot of linear piezoelectric motor researches focused on the stator structure design method, because the stator structure of the piezoelectric linear motors has

Huixia Zhang and Xifu Chen contributed equally

✉ Qian Lu
jackeylu@126.com

✉ Sungki Lyu
sklyu@gnu.ac.kr

¹ School of Mechanical Engineering, Yancheng Institute of Technology, Yancheng 224051, China

² School of Mechanical and Ocean Engineering, Huaihai Institute of Technology, Lianyungang 222005, China

³ School of Mechanical and Aerospace Engineering, ReCAPT, 501, Gyeongsang National University, Jinju-daero, Jinju-si, Gyeongnam-do 52828, Korea

a significant influence on the dynamic characteristics of the motor and the motor performance. A kind of motor stator, with feature of a flexible stator structure and piezoelectric stacks actuation, could simplify the motor structure and improve the operational stability of the motor, and it also could exhibit good application potential in large stroke and high precision occasions [19, 20]. The flexible stator structure design of the above motor was related to the dynamic output characteristics of the motor stator and the motor output performance. Therefore, many scholars have designed and optimized the corresponding flexible stator structure in detail [21, 22]. Sun et al. [23] proposed a novel double-foot piezoelectric linear motor with lever amplification mechanism, at the same time, the design process of the driving unit and the lever mechanism was described and analyzed. A linear piezoelectric motor with two parallel beams and two multilayer piezoelectric actuators was developed and the flexible beams were discussed [24].

In this paper, a flexible pentagon structure and two symmetrically arranged piezoelectric stacks were used to obtain an elliptical motion trajectory at the driving tip. Then the structural parameter of the motor stator was improved to enhance the motor performance.

2 Structure Principle of Flexible Drive-Foot

2.1 Displacement Characteristics of Five-Bar Mechanism

Figure 1 was a schematic diagram of the flexible five-bar mechanism with two degree of freedom, where, δ_1 and δ_2 are the output displacement of two piezoelectric stacks, respectively. In Fig. 1, the solid lines represent the original position of the five-bar mechanism, in which point C is the drive-tip. While the above two displacements were applied on the points P₁ and P₂, the displacements would be

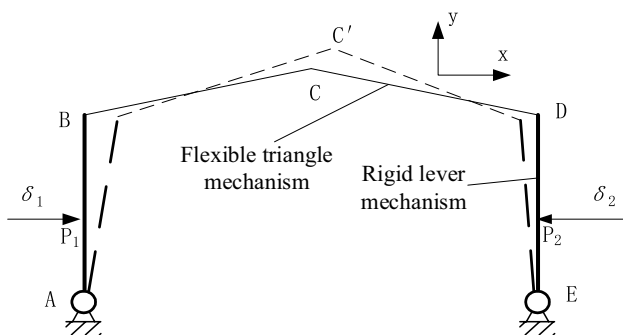


Fig. 1 The displacement schematic of flexible five-bar mechanism. AB and DE represent rigid lever, BCD is a flexible triangle. δ_1 and δ_2 represent the displacement excitation on the points of P₁ and P₂

produced at point C. The dotted lines represent the position after deformation.

Since the input displacements were tiny deformations, the displacements at B and D could be viewed as approximate horizontal displacements. While the piezoelectric stacks were excited by two sinusoidal voltages with the phase difference of $\pi/2$ and with the same amplitude. The input displacements can be expressed as Eq. (1).

$$\begin{cases} \delta_1 = A \sin \omega t \\ \delta_2 = A \cos \omega t \end{cases} \quad (1)$$

where A is the displacement amplitude of piezoelectric stacks.

2.2 The Formation of Elliptical Trajectory at Drive-Tip

In Fig. 2, it showed the movement of the drive-tip in one cycle, where, γ and γ' are the X displacement coefficients and the Y displacement coefficients at drive-tip in Fig. 2. Both γ and γ' are related to both the geometric size of flexible triangle mechanism and that of rigid lever mechanism. The displacements at drive-tip can be expressed as Eq. (2).

$$\begin{cases} x_c = \gamma(\delta_1 - \delta_2) \\ y_c = \gamma'(\delta_1 + \delta_2) \end{cases} \quad (2)$$

Thus, the elliptical motion trajectory can be obtained at drive-tip, and the equation of the trajectory was shown as Eq. (3), in which x_c and y_c are the displacement of drive-tip in x direction and in y direction, respectively. Therefore, the five-bar mechanism could be a kind of effective piezoelectric motor stator.

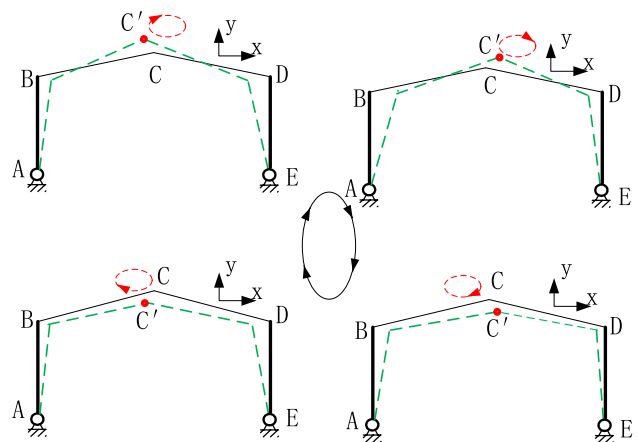


Fig. 2 The elliptical trajectory of drive-tip. The solid lines represent the original position and the dotted lines represent the position driven by the above displacement excitations. The red arrows represent the motion state of drive-tip in a whole sine exciting cycle

$$\frac{x_C^2}{2\gamma^2 A^2} + \frac{y_C^2}{2\gamma'^2 A^2} = 1 \tag{3}$$

3 Structural Design of Flexible Drive-Foot

3.1 Flexible Drive-Foot Structure

The flexible drive-foot included two flexible hinges, two cantilevers and a flexible triangle, and it was shown in Fig. 3. The flexible hinge lever mechanism can provide the lateral displacement output of the piezoelectric stacks. Meanwhile, the flexible triangle can convert the lateral displacement into the normal displacement at drive-tip.

In Fig. 3, some symbols could be defined as follows: t —the minimum thickness of the flexure hinges; R —the radius of the flexure hinges; L —the length of the cantilever; D —the length of the lever arm; θ —the bottom angle of the flexible triangle; b —the thickness of the flexible triangle;

When certain displacement loads in x direction was applied to the lever arm, two amplified displacements in both x and y directions can be obtained at drive-tip. Initially, based on the displacement amplification relationship and the design experience of the flexible structure [25], we determined the values of the above parameters as shown in Table 1.

3.2 Overall Structure of Motor Stator

On the basis of the prototype, the symmetrical structure design of motor stator was proposed. The stator of the motor comprised a drive-foot and a fixing device (including adjuster bolt and gasket), left piezoelectric stack and its preload mechanism (including the left side of the piezoelectric stack 1, wedge 1 and preloading bolt 1), right piezoelectric stack and its preload mechanism on the right side

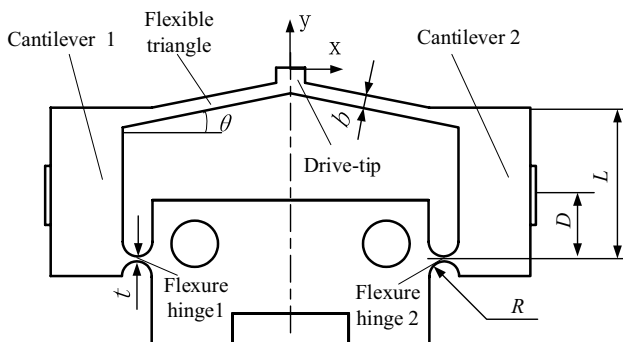


Fig. 3 The structure and main parameters of drive-foot. Cantilever s are corresponding to rigid levers. D and L are corresponding to the length of P_2E and the length of DE in Fig. 1, respectively

Table 1 Structural parameters of the drive-foot

Parameters	Value (Units)	Parameters	Value (Units)
b	0.8 (mm)	L	12 (mm)
θ	12 ($^\circ$)	R	1 (mm)
D	6 (mm)	t	1 (mm)

(including the left side of the piezoelectric stack 2, wedge 2 and preloading bolt 2). The motor stator structure was shown in Fig. 4.

In order to avoid the shear stress and tensile stress of piezoelectric stack in high frequency operation, it is necessary to design the support structure and preload mechanism of piezoelectric stack. In Fig. 4, the stator of the motor adopted a flexible parallel connecting rod mechanism and a wedge preload mechanism to realize the clamping and preloading of the piezoelectric stack.

As is known to all, the multilayer piezoelectric ceramics can endure little shear stress. Therefore, while the piezoelectric stack was preloaded, the direction of the preload should be parallel to the thickness direction of piezoelectric stacks. Therefore, a flexible displacement parallel mechanism (FDPM) was designed for transferring the displacement parallel to the thickness direction of the piezoelectric stacks, as shown in Fig. 5.

If the force F_x was applied to FDPM, the displacement δ_x in x direction would be produced, as shown in Fig. 5. When F_x was a constant, δ_x was dependent on l and t . Therefore, the relationship between the ratio of l/t and δ_x could be simulated by finite element method. Supposing that $F_x = 36$ N, the simulation results were shown in Fig. 6. The results show that the δ_x increased approximately exponentially with the increase of l/t .

By Ref. [23], the displacement loss of the micro displacement lever mechanism was proportional to $(l/t)^3$. Therefore, the larger the l/t was, the lower the output precision of the drive-tip was. Usually the value of (l/t) ranges from 2 to 4, consequently, we could set that: $l = 10.5$ mm, $t = 5$ mm.

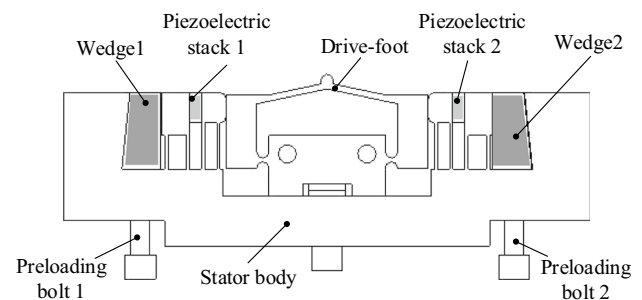


Fig. 4 Overall structure of the motor stator. The piezoelectric stacks are used to produce the input displacements. The wedges and preloading bolts are used for adjusting the preload of piezoelectric stacks

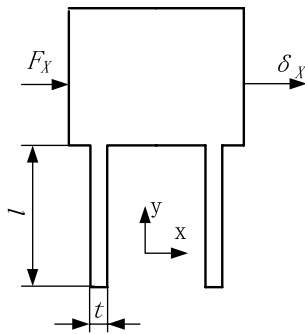


Fig. 5 The structure of flexible displacement parallel mechanism (FDPM). While a lateral force F_x applied to FDPM, a lateral displacement δ_x will be produced

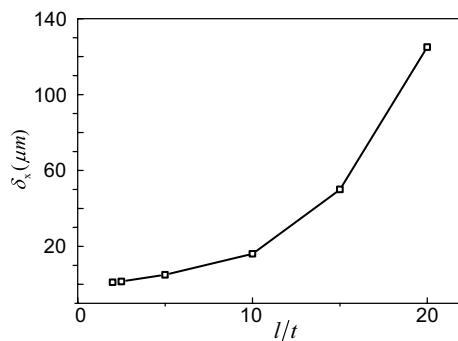


Fig. 6 Displacement simulation curve of FDM. The applied force F_x is 36N, the ratio of l/t range from 2 to 20

4 Improvement on Structural Parameter of Drive-Foot

4.1 The Finite Element Model of Drive-Foot

The simulation and analysis of the drive-foot were carried out by using finite element software. The material property definitions of the drive-foot are as follows: the elastic modulus (young's modulus) is 2.09×10^{11} Pa, the Poisson's ratio is 0.269, and the density is 7890 kg/m^3 . In order to improve the analysis accuracy, the unit size of the mesh for the drive-foot is 1 mm, and the unit size of the flexible triangle and flexible hinges is 0.5 mm. The results of the meshing are shown in Fig. 7a.

The drive-foot acted as a mechanism for energy conversion and transmission in the linear piezoelectric motor. Therefore, its mechanical characteristics directly affected the output performance of the motor. In order to simulate the mechanical properties that were acted by two piezoelectric stacks, two displacement loads of $3 \mu\text{m}$ were applied in position A and position B, respectively, which were shown in Fig. 7b. At the same time, the fixed constraints were applied

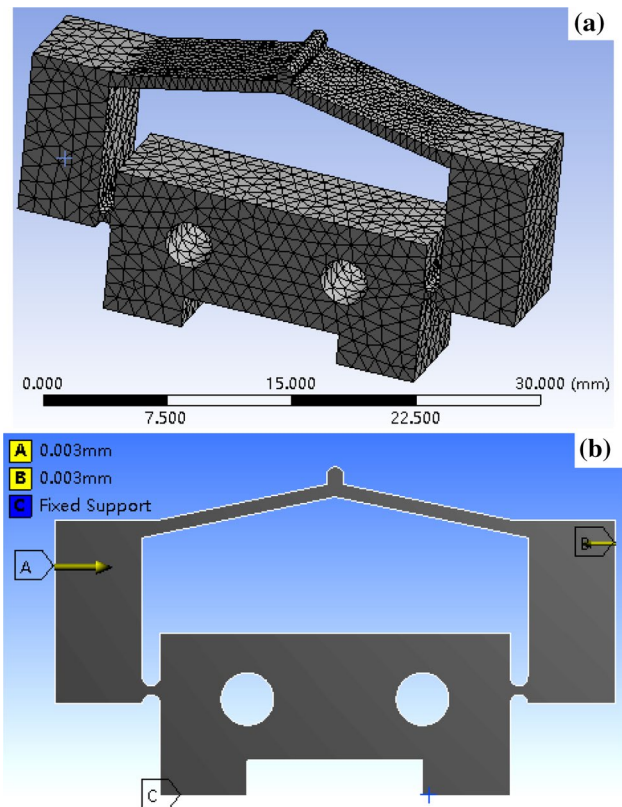


Fig. 7 The finite element model of drive-foot. **a** Finite element model with meshing; **b** boundary conditions and loads. The loads are applied on the position of A and B. The fixed boundary are set to point C

in the position C, which represented two bottom surfaces, as shown in Fig. 7b.

4.2 The Finite Element Simulation

In principle, the longitudinal amplitude of drive-tip and the stiffness of drive-foot would affect the output characteristics of the motor. Meanwhile, both the longitudinal amplitude of drive-tip and the stiffness of drive-foot are significant relative to the value of θ and b . Therefore, the simulation was carried out to find out the relations between the stiffness of drive-foot and the two parameters. Figure 8 shows the stiffness of drive-foot varies with θ under different values of b . It can be seen that when b is a constant, the stiffness of drive-foot decreases with the increase of θ . However, the stiffness of drive-foot increases with the increase of b , when θ is exactly the same. Obviously, when θ is in the right side of the flat line, the stiffness curves exhibit gentle change with θ . On the contrary, the stiffness decreases dramatically with the increase of θ . Basically, large stiffness can enhance the motor thrust and reduce the longitudinal amplitude of drive-tip. Therefore, choosing a proper stiffness of drive-foot is important for the motor.

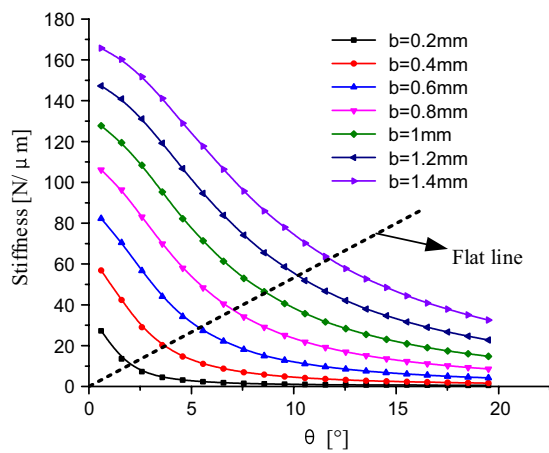


Fig. 8 The stiffness of drive-foot varies with θ under different value of b . The value of b varied from 0.2 to 1.4 mm. Flat line is the boundary line for the trend of stiffness via θ

By changing the values of θ and b , the change of the normal displacement amplitude can be obtained, as shown in Fig. 9. It can be seen that when b is a constant, the normal displacement amplitude of the drive-foot firstly increases with the increase of θ , and then decreases. While θ is between 1.5° and 5.5° , the longitudinal amplitudes of the drive-tip are in an optimal range.

When θ is the same, the normal displacements of the driving tip decrease as the thickness b increases. When $b < 0.2$ mm, there is a significant increase in the deformation of the drive-foot, that is to say, the structure of the drive-foot is too soft to be unstable. When $b > 1.4$ mm, the normal displacement amplitude of the output end changes little and tends to be stable, that is, the drive-foot tends to be a rigid structure.

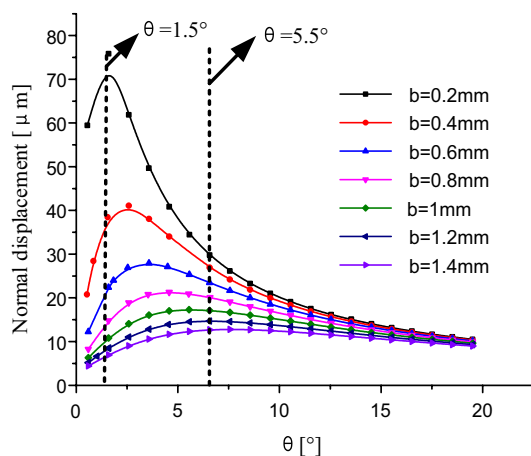


Fig. 9 The normal displacements of the driving tip varies with θ under different value of b . $\theta = 1.5^\circ$ and $\theta = 5.5^\circ$ is the boundary line for optimal interval of normal displacement

4.3 Improvement on the Structure Parameter of Drive-Foot

In order to improve the mechanical properties of the motor, we expect large normal displacement and large stiffness. However, the greater the stiffness is, the smaller the normal displacement is. Therefore, we expect to obtain a value of balanced stiffness and normal displacement, so that the mechanical properties of the motor approach to the optimal values. Based on the simulation curves in Figs. 9 and 10, both the values of θ and b have significant effects on the normal displacement of drive-tip and the stiffness of drive-foot. Therefore, it is difficult to find the optimal values of θ and b directly from Figs. 9 and 10. Considering that the longitudinal amplitude significantly influences the operational stability and output force of the motor, we use the normal displacement as the main improvement indicator. Thus, the optimal value of θ can be firstly determined by Fig. 9. Then the optimal values of normal displacement were obtained from the curves in Fig. 9 according to the optimal value of θ . Finally, the corresponding values of stiffness were derived from the curves in Fig. 10 according to the optimal value of θ .

Employing the above method, the optimal values of θ , the corresponding stiffness and the optimal normal displacement were produced under different values of b , as shown in Table 2.

According to Table 2, the curves of the optimal values of θ , the corresponding stiffness and the optimal normal displacement can be obtained, as shown in Fig. 10. From Fig. 10, it can be seen that with the increase of b , θ and the stiffness increase, but the normal displacement decrease. Usually, larger longitudinal amplitude of drive-tip results in higher thrust and higher stability of the motor, and the larger

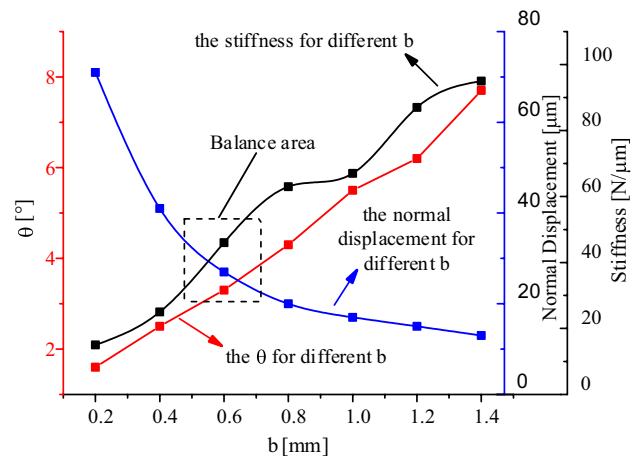


Fig. 10 The improved characteristic curves of the motor under different value of b . The balance area is determined by the stiffness curve and the normal displacement curve

Table 2 The improvement values of drive-foot for different b

Parameters (Units)	b (mm)						
	0.2	0.4	0.6	0.8	1	1.2	1.4
θ ($^{\circ}$)	1.6	2.5	3.3	4.3	5.5	6.2	7.7
Longitudinal amplitude (μm)	71	41	27	20	17	15	13
Stiffness ($\text{N}/\mu\text{m}$)	15	25	46	63	67	87	95

Table 3 The characteristic comparison of drive-foot

Parameters (Units)	b (mm)	θ ($^{\circ}$)	Longitudinal amplitude (μm)	Stiffness ($\text{N}/\mu\text{m}$)
Before optimization	0.8	12	14.7	19
After optimization	0.6	4	23.3	35

stiffness of drive-foot contributes to higher thrust. Therefore, there exists a balance area, as shown in Fig. 10, where both stiffness and normal displacement are not too small. In the balance area, b ranges from 0.5 to 0.7 mm, and θ is from 3° to 5° . Thus we determine the parameters as the following: $\theta = 4^{\circ}$, $b = 0.6$ mm.

Further, the improved drive-foot was modified and simulated. Then the normal displacement of drive-tip and the stiffness of the improved drive-foot could be obtained as shown in Table 3.

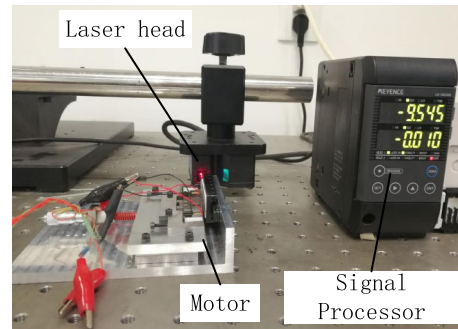
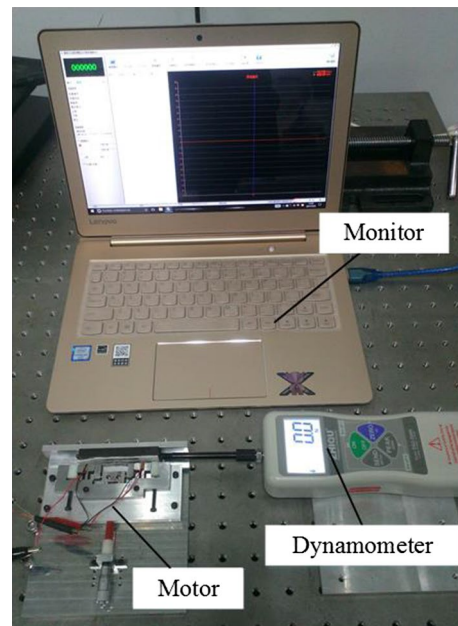
Compared with the simulation results before improvement, the stiffness of the improved driven foot is $35 \text{ N}/\mu\text{m}$, which can meet the requirements of the piezoelectric stack to drive the drive-foot. The normal displacement amplitude of the drive-foot is $23.3 \mu\text{m}$, which is increased by 58.5% compared with that before improvement.

5 Experimental Research

According to the above results, both un-improved drive-foot and improved drive-foot were processed and two different piezoelectric motors were fabricated. The test devices for displacement tests and thrust tests of the motors were shown in Figs. 10 and 11, respectively.

During the assembly of motor stator, the symmetry of the piezoelectric stacks, and the verticality of both sides of the drive-foot, which is relative to the lower end face of the support, should all be guaranteed. When the motor was assembled, the stator clamping device needed to be precisely adjusted to ensure the good contact between the drive-tip and the vibrator (Fig. 12).

Figure 13 shows the motion characteristics of the motors at an excitation voltage of 140 V. Compared with the un-improved motor, the optimized motor can work in lower frequency. The operating frequency range of the

**Fig. 11** The picture of displacement test devices. Laser head is used to test the displacement of drive-tip**Fig. 12** The picture of thrust test devices. Dynamometer is used to test the motor thrust with the resolution of 0.1 N

improved motor is from 900 to 1900 Hz, while that of the un-improved motor is from 3200 to 4200 Hz. The maximum velocity of the two motors is both nearly 2.55 mm/s . It can be seen from Fig. 13 that as the frequency increase, the speed of the motor firstly increases and then decreases. For the both motors, maximum motor velocity were obtained under an optimal frequency.

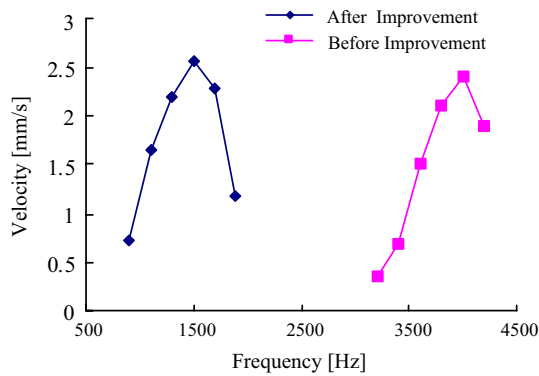


Fig. 13 The motor velocity versus frequency. Due to the larger stiffness of the improved motor, it runs in a lower frequency range

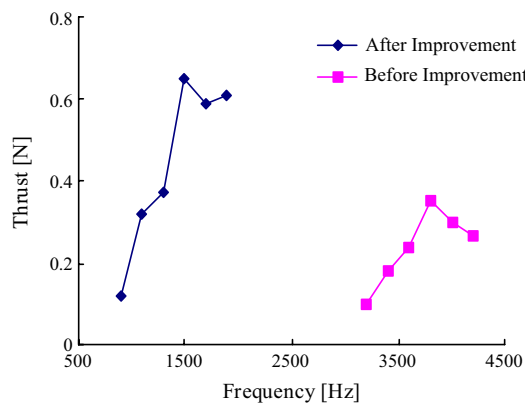


Fig. 14 Thrust of the motors versus frequency. Due to the larger stiffness and the larger normal displacement of the improved motor, its maximum thrust is larger

Figure 14 shows the thrust characteristics of the motors under different frequencies. And it can be seen from Fig. 14, with the increase of the frequency, the thrust of the both motors increase firstly and then decrease. When the frequency is 1500 Hz and 3500 Hz, the improved motor and the un-improved motor reach the highest thrust of 0.64 N and 0.42 N, respectively.

According to the test results, the properties of the motors could be summarized, which was shown in Table 4.

According to the motor test results, the output force of the motor is increased by 52.38% compared with that before optimization. This is because the increase of the stiffness of drive-foot and the normal displacement of drive-tip can increase the normal pressure between the stator and the slider. Theoretically, the velocity is independent to the stiffness of drive-foot and the normal displacement of drive-tip. Therefore, the velocity is hardly affected by the optimization.

The speed-load characteristics were studied with the method of hanging weights at one end of the slider, as shown

Table 4 Comparison of output performance between initial motors and optimized motor

Indicators (Units)	Thrust (N)	Velocity (mm/s)	Efficiency (%)
Before improvement	0.42	2.54	9.40
After improvement	0.64	2.56	23.96
Increased percentage	52.38%	0.79%	159.15

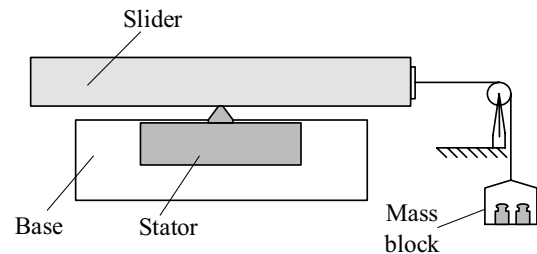


Fig. 15 Experimental system schematic of the load speed characteristic. While change the mass of mass block, the velocity can be tested for different load

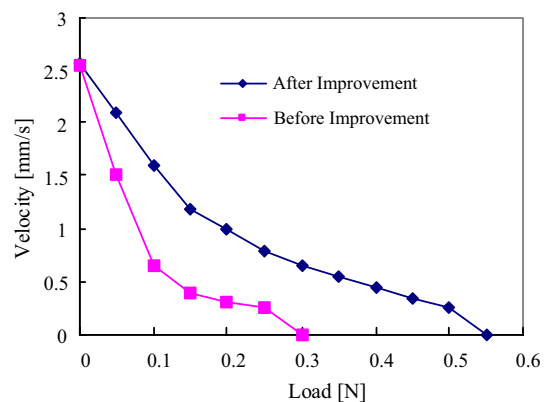


Fig. 16 The velocity–load characteristic of motors. The no-load velocity of the both motors. The maximum thrust of the improved motor is large than that of the un-improved motor

in Fig. 15. When the exciting frequency is the optimal frequency and the exciting voltage is 140 V, the velocities of the motor were tested with different loads, and the speed-load curves were shown in Fig. 16.

6 Conclusion

By establishing the drive-foot structure model, the equation of elliptic motion trajectory at the drive-tip was derived. It is proved theoretically that the motor with flexible drive-foot can operate steadily in a wide frequency range. The simulation of the drive-foot structure by using finite element software, and the simulation results show that the

magnification of drive-foot is greatly affected by the bottom angle and the thickness of the flexible triangle. In order to improve the output performance of the motor, the normal displacement amplitude of the drive-tip is increased, and the structural parameters of the drive-foot are optimized. According to the simulation results, the stiffness of drive-foot is increased by 84.21% and the normal displacement amplitude of the drive-tip is increased by 58.50% through the improved design. Experiment results of motor characteristic show that the thrust of motor is increased by 52.38% and the maximum velocity nearly unchanged. Particularly, this type of piezoelectric motor has the advantages of simple structure and good operational stability. And it can realize the stroke of 200 mm and an open-loop displacement resolution of 0.05 μm .

Acknowledgements This work was a project funded by the National Natural Science Foundation of China (Number: 51405420, 51375224, 51805465); Youth project of Jiangsu Natural Science Foundation of China (Number: BK20140474); Natural Science Research Projects in Jiangsu Higher Education Institutions (18KJB460030); Qing Lan Project of Jiangsu Higher Education of China (Su-Teacher 2018-12); The sponsorship of Jiangsu Oversea Research and Training Program for University Prominent Young & Middle-aged Teachers.

References

- Boldea, I., Tutelea, L., & Xu, W. (2017). Linear electric machines, drives and MAGLEVs: An overview. *IEEE Transactions on Industrial Electronics*, *99*, 1–2.
- Uchino, K. (2011). *Piezoelectric actuators and ultrasonic motors*. New York: Springer Publishing Company, Incorporated.
- Wang, L., Wielert, T., & Twiefel, J. (2017). A rod type linear ultrasonic motor utilizing longitudinal traveling waves: Proof of concept. *Smart Materials and Structures*, *26*, 1–9.
- Ci, P., Liu, G., & Chen, Z. (2013). A standing wave linear ultrasonic motor operating in face-diagonal-bending mode. *Applied Physics Letters*, *103*, 1033.
- Kotani, H., Takasaki, M., & Mizuno, T. (2016). Surface acoustic wave linear motor using glass substrate. *Journal of the Japan Society for Precision Engineering*, *82*, 239–242.
- Suleman, A., Burns, S., & Waechter, D. (2014). Design and modeling of an electrostrictive inchworm actuator. *Mechatronics*, *14*, 567–586.
- He, L., Chu, Y., & Hao, S. (2018). Inertial piezoelectric linear motor driven by a single-phase harmonic wave with automatic clamping mechanism. *Review of Scientific Instruments*, *89*, 055008.
- Kümmel, M., Goldschmidt, S., & Wallaschek, J. (1998). Theoretical and experimental studies of a piezoelectric ultrasonic linear motor with respect to damping and nonlinear material behavior. *Ultrasonics*, *36*, 103–109.
- Xiang, L., Yao, Z. Y., & Zhou, S. (2016). Dynamic modeling and characteristics analysis of a modal-independent linear ultrasonic motor. *Ultrasonics*, *72*, 117–127.
- Lu, F., Lee, H. P., & Lim, S. P. (2001). Modeling of contact with projections on rotor surfaces for ultrasonic traveling wave motors. *Smart Materials and Structures*, *10*, 860.
- Fang, J. W., Zhang, L. F., Long, Z. L., et al. (2018). Fuzzy adaptive sliding mode control for the precision position of piezo-actuated nano positioning stage. *International Journal of Precision Engineering and Manufacturing*, *19*, 1447–1456.
- Lin, C. M., & Li, H. Y. (2014). Intelligent control using the wavelet fuzzy CMAC backstepping control system for two-axis linear piezoelectric ceramic motor drive systems. *IEEE Transactions on Fuzzy Systems*, *22*, 791–802.
- Olyaie, M. S., Razfar, M. R., & Wang, S. (2011). Topology optimization of a linear piezoelectric micromotor using the smoothed finite element method. *Computer Modeling in Engineering & Sciences*, *82*, 55–81.
- Li, C., & Xing, J. (2018). Dynamic optimization of an electro-mechanical integrated harmonic piezoelectric motor. *Journal of Mechanical Science and Technology*, *32*(6), 2517–2526.
- Ko, H. P., Kim, S., & Kang, C. Y. (2005). Optimization of a piezoelectric linear motor in terms of the contact parameters. *Materials Chemistry and Physics*, *90*, 322–326.
- Yu, H., Quan, Q., & Tian, X. (2018). Optimization and analysis of a u-shaped linear piezoelectric ultrasonic motor using longitudinal transducers. *Sensors*, *18*, 809.
- Aminzahed, I., Mashhadi, M. M., & Sereshk, M. R. V. (2017). Investigation of holder pressure and size effects in micro deep drawing of rectangular work pieces driven by piezoelectric actuator. *Materials Science and Engineering C*, *71*, 685–689.
- Aminzahed, I., Mashhadi, M. M., & Sereshk, M. R. V. (2015). Influence of drawn radius in micro deep drawing process of rectangular work pieces via size dependent analysis using piezoelectric actuator. *International Journal on Interactive Design and Manufacturing (IJIDeM)*, *11*, 893–902.
- Funakubo, T., Tsubata, T., & Taniguchi, Y. (2014). Ultrasonic linear motor using multilayer piezoelectric actuators. *Japanese Journal of Applied Physics*, *34*, 2756–2759.
- Yuan, S., Zhao, Y., & Chu, X. (2016). Analysis and experimental research of a multilayer linear piezoelectric actuator. *Applied Sciences*, *6*, 225.
- Wang, H., Zhang, Y., & Li, Z. (2014). A V-shaped small linear ultrasonic motor with multilayered piezoelectric stacks. *Indian Journal of Engineering & Materials Sciences*, *21*, 495–500.
- Saigoh, H., Kawasaki, M., & Maruko, N. (1995). Multilayer piezoelectric motor using the first longitudinal and the second bending vibrations. *Japanese Journal of Applied Physics*, *34*, 2760–2764.
- Sun, M., Huang, W., & Wang, Y. (2017). Research on a novel non-resonant piezoelectric linear motor with lever amplification mechanism. *Sensors and Actuators, A: Physical*, *261*, 302–310.
- Aoyagi, M., Nakayasu, R., & Kajiwara, H. (2016). Non-resonance type linear ultrasonic motor using multilayer piezoelectric actuators with parallel beams. *International Journal of Automation Technology*, *10*, 557–563.
- Zheng, W. Z., & Xin, H. B. (2003). Analysis of displacement loss in micro displacement magnification mechanism. *Journal of Machine Design*, *20*, 25–26.

Publisher's Note Springer Nature remains neutral with regard to jurisdictional claims in published maps and institutional affiliations.



Xifu Chen Ph.D., Associate professor in Yancheng Institute of Technology. His research interest is piezoelectric actuators and precision mechanism design. E-mail: chenxifyou@163.com.



Qian Lu Ph.D., Associate professor in Yancheng Institute of Technology. His research interest is compliant mechanism and piezoelectric driving technology. E-mail: jackeylu@126.com.



Ming Li Master Candidate in Yancheng Institute of Technology. His research interest is piezoelectric motors. E-mail: 460540661@qq.com.



Sungki Lyu Professor in the Department of Mechanical Engineering, Gyeongsang National University. His research interest is Mechanical System Design. E-mail: sklyu@gnu.ac.kr.



Huixia Zhang Associate professor in Huaihai Institute of Technology. Her research is Ultrasonic motors & Add material manufacture & Surface modification. E-mail: hxzhang2011@163.com.